

# Low Frequency 1/f Noise on QWIPs, nBn, and Superlattice Focal Plane Array

S. B. Rafol, S. D. Gunapala, D. Z. Ting, A. Soibel, C. J. Hill, A. Khoshakhlagh, S. A. Keo, A. Fisher, J. K. Liu, J. M. Mumolo, and B. Pepper

Center for Infrared Photodetectors, Jet Propulsion Laboratory, California Institute of Technology  
4800 Oak Grove Drive, Pasadena, CA 91109, USA

## ABSTRACT

Noise Equivalent Difference Temperature (NE $\Delta$ T) is a standard performance metric for most infrared focal plane array (FPA) systems. The frequency bandwidth and range associated with NE $\Delta$ T is normally at high frequency and it does not describe the long time noise behavior or the very low frequency noise of the FPA. Very low frequency noise measurement requires data capture that takes longer time duration and sampling interval. This study investigates low frequency noise in QWIP, nBn and LWIR n-type Complementary Barrier Infrared Detector (CBIRD) FPAs. The corner frequencies are extracted from the power spectral density (PSD) as function of frequency. The peak wavelength, quantum efficiency of QWIP detector are 6.2  $\mu$ m and 2 %, respectively. QWIP FPA has a mean NE $\Delta$ T  $\sim$  25 mK at an operating temperature of 65 K and an integration time of 16 msec. The mean QWIP PSD plot shows a corner frequency of  $<$  0.5 mHz. The nBn FPA with 4  $\mu$ m cut off and quantum efficiency of 67 % has NE $\Delta$ T  $\sim$  15.6 mK at an integration time  $\sim$  7.52 msec and an operating temperature of 120 K. The nBn has corner frequency of  $>$  50 mHz. Lastly the n-type CBIRD FPA with a 50% cutoff at 8.8  $\mu$ m and quantum efficiency of  $\sim$  50 % has an NE $\Delta$ T  $\sim$  18.6 mK at an integration time of 1.86 msec and operating temperature 120 K. The superlattice FPA has a corner frequency  $\sim$  10 mHz. The investigation of the tail on the NE $\Delta$ T histogram reveals that its origin is not accounted for entirely by the high noise current, but also it needs the inclusion of lower responsivity for some pixels.

**Keywords:** infrared detector, QWIP, nBn, CBIRD focal plane array, 1/f noise

## Introduction

Many electronic devices have inherently low frequency noise. Normally these devices operate at some defined frequency bandwidth. Unfortunately for many systems the lower frequency limit is within the range of low frequency noise related to 1/f noise (flicker noise). This is the case for CMOS imager [1,2] and many II-VI infrared detector systems [3,4]. 1/f noise was first described by Johnson in 1925.[5] The presence of 1/f noise at lower frequencies is an unwanted device electrical behavior since it degrades the performance. It is of interest to avoid these low frequency entirely. But for some system this is not possible. For infrared camera system this 1/f noise is an unwanted consequence and it has to be minimized to avoid artifacts. Detector is at the front-end of many infrared systems and it is preferable that the detector noise is the most dominant in comparison to subsequent stages in the system. This ensures that the system is detector noise-limited and it is the most ideal mode of operation. It is important to minimize the effect of noise in general, including 1/f noise at the detector and read out integrated circuit (ROIC). FPA is a

hybrid of detector array and ROIC. The very close proximity of the first stage amplifiers on the ROIC to detector array reduces noise pick up and the amplified analog output signal at the low-impedance output is quite easy to interface with standard electronic components with noise less than the minimum noise associate with ROIC.

Experimental investigation of the physical origin of  $1/f$  noise is important, especially for infrared FPA. Power spectral density (PSD) in the frequency domain is a tool to illustrate a frequency range where different noise sources are dominant [6,7]. At higher frequency, PSD is normally frequency-independent, and it is dominated by white noises. These are shot and thermal noise [8] which cannot be completely suppressed and their effect can be minimized by limiting frequency bandwidth of system to decrease the integrated noise power. The frequency plot of PSD versus frequency typically shows the presence of  $1/f$  noise at lower frequency in most photon detectors. Generally it is an inverse relation of a form  $\sim 1/f^\alpha$ , where  $\alpha \geq 1$ . Understanding the sources of fluctuations can assist in the design of high performance and low noise infrared detector system. Theoretical foundation of  $1/f$  noise is still lacking. The corner frequency  $f_c$  can be defined as the frequency location where PSD( $f$ ) starts to increase with inverse frequency.  $f_c$  can be interpreted as a transition from a high frequency PSD dominated by noises from all current sources to lower frequency PSD dominated by  $1/f$  noise. The  $f_c$  value can be considered a figure of merit for infrared camera system since it can be related to temporal stability and how often to refresh the calibration table.[9] Hence a lower  $f_c$  value is preferred.

The simplest way to view the  $1/f$  noise is through a conductivity relation ( $\sigma = en\mu$ ) which is proportional to the product of charge carrier density ( $n$ ) and mobility ( $\mu$ );  $e$  is the electronic charge. Either  $n$  or  $\mu$  can fluctuate and can result to  $1/f$  noise behavior. The mobility fluctuation model was first proposed by Hooge, et. al.[10] It attributes  $1/f$  noise to lattice impurity scattering as well as to other scattering processes. Carrier density fluctuation can also lead to  $1/f$  noise. This is believed to be due to random trapping/detrapping of charge carriers.[11] This type of behavior assumes that  $1/f$  completely occurs internally inside the device and external influence is suppressed. This basically means a thermally and mechanically closed system. But for most infrared camera systems, it is not a completely closed system where energy flow is restricted; external influence can contribute to  $1/f$  noise. For example, temperature fluctuation of the camera window can manifest as  $1/f$ -noise like behavior if observed for a long time. This paper reports on the  $1/f$  noise of infrared detector system based on III-V compound semiconductors.

### **QWIP 640 x 512 Focal Plane Array**

A high performance 640 x 512 QWIP FPA was integrated into a dewar and cryocooler which become an integral component of the FLIR Phoenix camera. The ROIC is a FLIR/Indigo ISC9803 with a 25  $\mu\text{m}$  pixel pitch and fill factor is 85 %. The spectral band of this FPA has a peak wavelength of 6.2  $\mu\text{m}$  which only requires a temperature of operation at only  $\sim 71$  K. The camera electronics has a 14-bit digital resolution, and an  $f/2$  optics. Flat black body data at temperatures 295 K, 300 K and 305 K were taken to estimate the median NE $\Delta$ T  $\sim 25$  mK at an integration time of 16 msec and a 30 Hz frame rate. Figure 1 shows the NE $\Delta$ T histogram of the QWIP FPA. The NE $\Delta$ T histogram shows very little tail which implies that most pixels have no low frequency noise

down to  $\sim 0.5$  Hz which is related to time duration of the captured data. The spatial non-uniformity after correction is  $< 0.02\%$ . The approximate low and high frequency limit which defines the bandwidth for NE $\Delta$ T measurement are 0.5 Hz and 15 Hz respectively. Hence to sample lower frequency noises, a large amount of data need to be captured at 30 Hz frame rate, or alternatively, just capture frame at a larger time interval to reduce the data volume. The latter approach is chosen.

For low frequency noise measurement, the camera system electronic was allowed to warm up, and the FPA was given at least one hour for temperature stabilization. Since the aperture was not blocked, QWIP FPA was allowed to stare at the flat black body at 300 K temperature. Only the Ge-window material is between cold FPA and constant high emissivity flat black body surface. The window is assumed to be at room temperature. Data collection was conducted with detector off (no-bias) and detector on (bias). The detector-off data determine the noise behavior as a function of frequency of the ROIC. The pre-amplifiers and analog-to-digital converters are assumed to have low input referred noises. In this case, the detector-off limiting noise source is the ROIC. The measurement indicates that a VDETCOM bias of roughly 4 V set the detector bias at 0 V and VDETCOM at 5.6 V provides the optimum bias. The QWIP detector then has a biased of  $\sim 1.6$  V in normal operation. A data acquisition running LabVIEW is used to capture the Phoenix camera 14-bit RS422 uncorrected video output and to interface with the RS232 to control the camera configuration. The frame is captured at a time interval of  $\Delta T = 40$  seconds for a duration of two-and-half days for each bias (0 V and 1.6 V). The total data collection duration is five days.

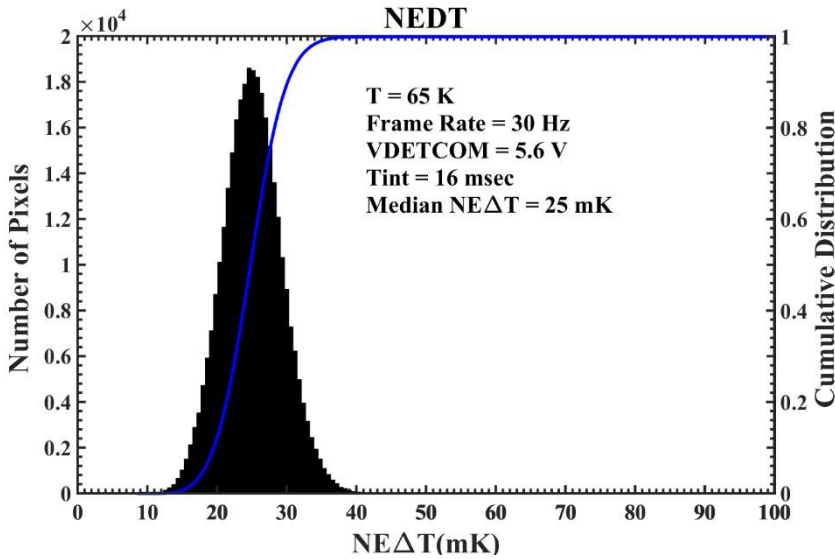


Figure 1. NE $\Delta$ T histogram of QWIP Phoenix camera. The FPA temperature is at 65 K.

Three time series data set were constructed from mean of the three regions, left 25x50 pixels, middle 40x50 pixels and right 60x50 pixels. The time series data elements are spatial averages of the three regions. This time series construction leads to linear array of data by collapsing a small region in a frame at a fixed time. The evolution time series is constructed by subtracting the first frame from all the subsequent frames and

then the time series data are constructed from the mean of each region defined by

$$d_i = (F_i - F_1), i = 1 : N, \quad (1)$$

where N is the total number of sampled frames and  $F_1$  is the first frame.

Alternatively, the mean time series can be constructed by subtracting the mean of all the frames from each frame.

$$d_i = (F_i - \bar{F}), i = 1 : N , \quad (2)$$

where  $\bar{F}$  is the mean frame of all frames. Smaller number of pixels in each region has been investigated also.

The single-sided PSD [12] as a function of frequency was calculated using

$$PSD(f) = 2 \frac{|FFT(d_i)|^2}{N\Delta t^{-1}} , \quad (3)$$

where  $FFT(d_i)$  is fast Fourier transform of the time series data.  $\Delta t$  is the sampling time and  $N$  is the total number of frames.  $PSD(f)$  can be described as a noise power variation versus frequency. It was concluded that the end result did not depend on how the time series was constructed (either by evolution or by mean method) since both approaches seemed to converge to the same  $PSD(f)$ . However, the  $PSD(f)$  from averaging smaller number of pixels seems to have slightly higher noise at higher frequency than the spatial average from a larger number of pixels. This is because spatial averaging on a single frame is similar to a temporal averaging of noise from single pixel.

The left hand side of Fig. 2 shows the  $PSD(f)$  for detector on and detector off. The detector off  $PSD$  is less than detector on  $PSD$ , indicating that the system has lower noise down to frequency  $< \sim 4 \times 10^{-5}$  Hz. At frequencies above  $\sim 4 \times 10^{-4}$  Hz, detector on  $PSD(f)$  is roughly four times higher than detector off  $PSD$ . This fulfills the desired condition that the detector must have higher noise at 300 K background temperature. The detector off  $PSD(f)$  is interesting since it shows that the electronic system also exhibits an increasing noise at low frequency. It is expected that when detector is off there is very low or no noise originating from the detector. This detector off behavior is expected since CMOS devices can also exhibit  $1/f$  noise [13] which may be due to a reset transistor. The right hand side of Fig. 2 shows the  $PSD(f)$  of just the detector which was estimated by taking the difference of detector on and detector off  $PSD(f)$  at each frequency. The  $PSD$  at lower frequency increases by two orders of magnitude from  $\sim 4 \times 10^{-4}$  Hz to  $4 \times 10^{-5}$  Hz and an  $f_c$  of  $< 0.5$  mHz is determined. Interestingly, this is comparable to  $f_c$  of both detector off and detector on  $PSD(f)$ . This implies that the ROIC and the electronics do not alter the  $f_c$ . Ressler et. al. [14] reported an  $f_c \sim 10$  mHz for 8-9  $\mu\text{m}$  QWIP FPA and peak wavelength at  $\sim 8.5 \mu\text{m}$ . This is a factor of 20 higher, but it also has at a higher peak wavelength. The estimated  $1/f$  noise for the QWIP detector is assumed an upper limit since the contribution from external sources, such as window temperature drift, cryocooler induced noise and blackbody temperature fluctuation, are neglected and the detector on and detector off data were not taken simultaneously.

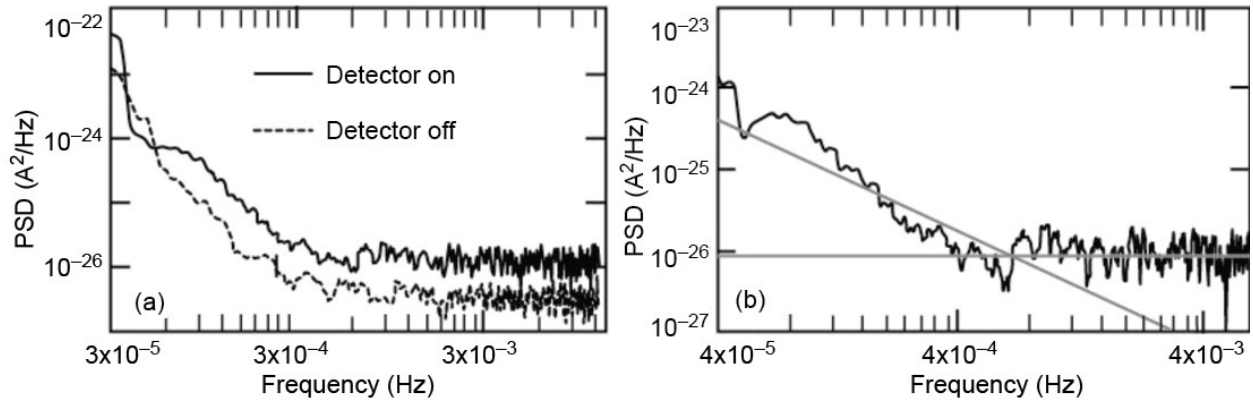


**Figure 2.** Left hand side is the QWIP FPA PSD versus frequency for detector off (no bias) and detector on (bias). Right hand side is the QWIP PSD versus frequency which is the difference of the PSDs of detector on and detector off.

### NE $\Delta$ T and 1/f NOISE OF nBn DETECTOR ARRAY

FPA based on nBn detectors are investigated for low frequency 1/f noise also. The device structure was first proposed by S. Maimon and G. W. Wicks [15]. These nBn devices were grown at JPL on 3-inch GaSb substrate with 4  $\mu$ m thick InAsSb absorber layer and AlAsSb barrier. The cut off wavelength at 120 K is  $\sim$  4  $\mu$ m and the measured quantum efficiency is  $\sim$  67%. Detectors arrays with 640x512 format were fabricated to match the 25  $\mu$ m pitch of FLIR/Indigo ISC9803 ROIC. Dry etching process was utilized for deep etching. This fully isolates each pixel from its neighbor to prevent electrical and optical crosstalk. There was no surface passivation on the side wall.

The nBn FPA was integrated with a  $\frac{1}{4}$  Watt low power micro cooler Ricor K561 with an f/2 cold aperture. The SEIR test system electronics is used to operate the FPA and has a 14-bit digital resolution. Flat black body data at temperatures 295 K, 300 K, and 305 K were taken to estimate the median NE $\Delta$ T at an integration time of 7.52 msec and 15 Hz frame rate. The left hand side of Fig. 3 shows the estimated NE $\Delta$ T histogram and the right hand side are the captured images at temperatures from 110 K to 170 K. At 120 K operating temperature a median NE $\Delta$ T value of 15.6 mK at bias 200 mV is determined. The NE $\Delta$ T distribution has very little tail toward higher NE $\Delta$ T values which implies that most pixels have very low noise and good responsivity value at lower frequency down to  $\sim$  0.23 Hz which is the lowest frequency content of the NE $\Delta$ T data. The 3 x median NE $\Delta$ T pixel operability is 99.6% which demonstrates the high FPA performance.

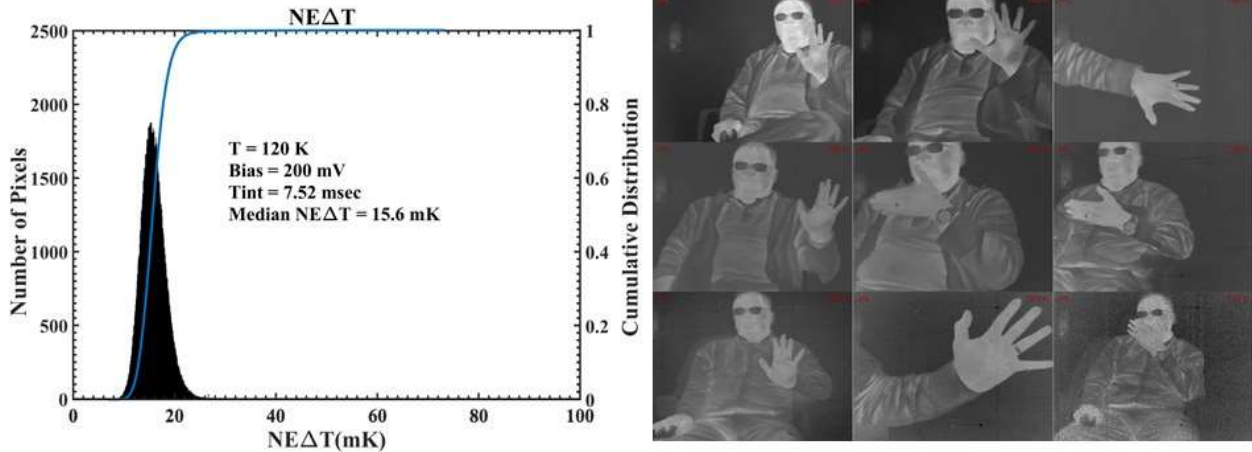


**Figure 3. nBn FPA NEDT histogram on the right and two-point corrected images from 110 K FPA temperature at the upper left corner to 170 K FPA temperature at bottom right hand corner.**

For  $1/f$  noise study, the method of data collection is similar to QWIP Phoenix camera previously described. An SEIR test system electronics was used to operate the nBn FPA at a fixed temperature and a separate computer running LabVIEW to capture frames at  $\Delta t = 2$  seconds interval. The camera system was allowed to warm up to stabilize the electronics and FPA temperature. The aperture is open, and the FPA was allowed to stare at a flat black body at 300 K temperature. Only the Si-window material is in the optical path between the cold FPA and a constant temperature flat black body. The operating parameters are: frame rate = 15 Hz, Integration time = 7.52 msec, and FPA temperature = 120 K. Since the ROIC is similar to QWIP FPA described above, the construction of the time series data is similar.

Figure 4 (a) shows the PSD( $f$ ) of the detector on (biased) and the detector off (un-biased). The detector off PSD( $f$ ) is from the ROIC and test system noise power contribution and the detector on PSD( $f$ ) is the sum of PSD( $f$ ) from the system and the detector at each frequency. Note that the detector-off has lower PSD( $f$ ) than detector-on PSD( $f$ ). The detector-on PSD above 50 mHz is  $> 30$  times larger than detector-off PSD. This indicates an almost ideal background limited condition and fulfills the condition that the camera system is detector noise limited at 300 K background temperature. The plot of the difference of detector on and detector off PSD( $f$ ) at each frequency is shown in Figure 4 (b), which is assumed to be from the detector PSD contribution only. For comparison, white noise (shot noise) from the dark and the photo current was estimated to be at  $\sim 1.9 \times 10^{-14}$  A. The dark current was measured at various temperatures in an LN2 dewar prior to a dewar and cooler integration. At higher frequency, PSD is roughly  $\sim 3 \times 10^{-27}$  A<sup>2</sup>/Hz. Assuming a 1 Hz frequency bandwidth, the estimated noise current from the PSD with 1 Hz frequency bandwidth is  $\sim 5.5 \times 10^{-14}$  A, which is higher than the estimated white noise from the dark and the photo current. These noise currents are higher than the estimated from read noise current  $\sim 1.2 \times 10^{-14}$  A of the ROIC using 7.52 msec integration time. One possible origin of the noise current discrepancy is cryocooler induced noise.

The corner frequency  $f_c$  is roughly between 50-90 mHz. This  $f_c$  is higher than QWIP FPA  $f_c$  with similar ROIC. This nBn  $f_c$  is comparable to the  $f_c$ 's from the detector off and detector on PSD(f). In addition, the micro cooler and driving electronics are different for the QWIP Phoenix camera and nBn which can influence the low frequency noise. Therefore detector off  $f_c$  from QWIP and nBn FPA do not have to agree. Also the high frequency PSD of detector off in QWIP is roughly  $\sim 2 \times 10^{-27} \text{ A}^2/\text{Hz}$ , which is higher than the nBn high frequency detector off PSD ( $\sim 10^{-27} \text{ A}^2/\text{Hz}$ ). The nBn detector PSD(f) at low frequency is assumed to be an upper limit since the contribution from external sources, such as temperature fluctuation from the window, cryocooler and black body, is neglected and the detector on and detector off data were not recorded simultaneously. Device related  $1/f$  behavior can also originate from the unpassivated detectors.[16]

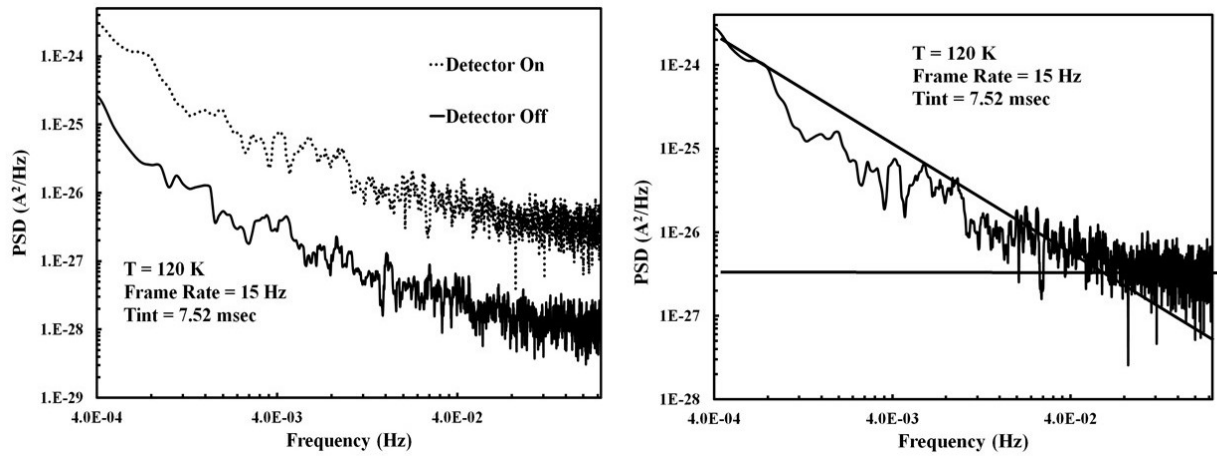


Figure 4. (a) PSD of nBn FPA with and without bias; (b) PSD of nBn detector which is the difference between with and without bias PSD on (a).

### NEDT and 1/f NOISE OF CBIRD DETECTOR ARRAY

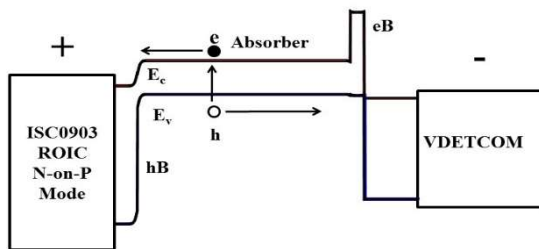
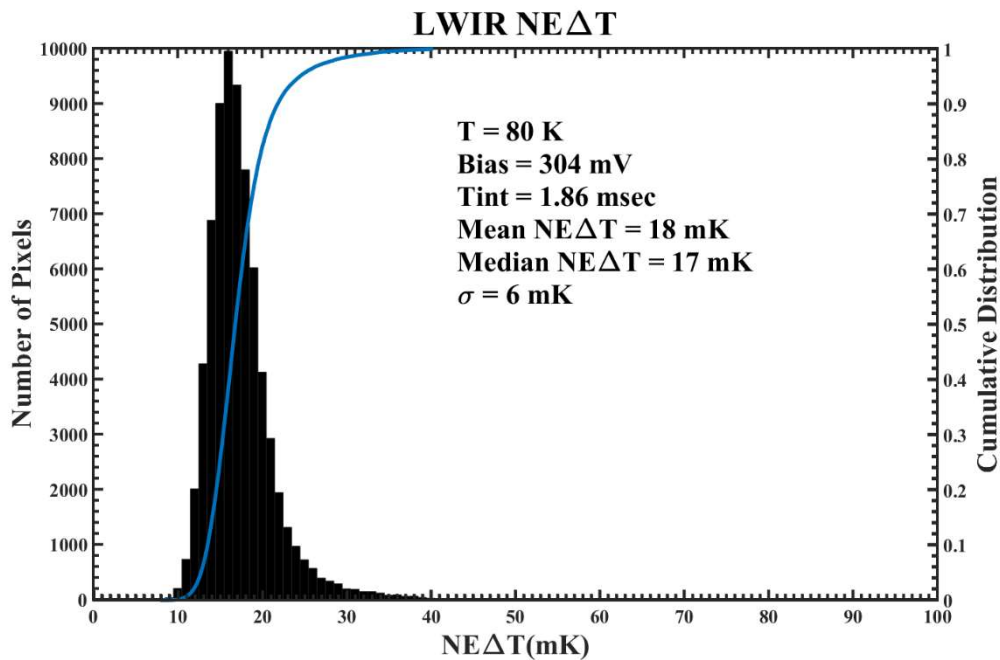


Fig 5. Energy band diagram of the n-CBIRD. Photons are absorbed and electrons diffuses towards the ROIC.

electrically connected to ISC0903 FLIR/Indigo ROIC.[19] The measured 50% cut-off is roughly  $\sim 8.8 \mu\text{m}$ . The hB and eB are respectively designed to have approximately zero conduction and valence band offsets with respect to the absorber. The absorber and eB are nominally doped n-type

An n-type Complementary Barrier Infrared Detector (CBIRD) [17,18] device structure was grown at JPL on GaSb substrate. It has a 300-period (44 Å, 21 Å)-InAs/GaSb absorber superlattice terminated on one side by an 80-period (46 Å, 12 Å)-InAs/AlSb hole-barrier (hB) superlattice and 60-period (22 Å, 21 Å)-InAs/GaSb electron-barrier (eB) superlattice on the other side. Fig 5 shows an n-type CBIRD device structure that is

at  $\sim 1 \times 10^{16} \text{ cm}^{-3}$ , while InAsSb next to eB is the VDETCOM layer. The hB is the other contact, which is electrically connected to the ROIC pixel unit cell. VDETCOM is the common contact for all pixels and it is at a fixed voltage. The detector arrays were etched all the way through the bottom contact, and no surface passivation was applied. For an n-type CBIRD, VDETCOM is at a lower potential with respect to the top contact which electrically interfaces with the ROIC. The mode of operation of the ROIC is n-on-p which injects electrons into the ROIC. The FLIR/Indigo 0903 is a two-color direct injection  $320 \times 256$  pixel format ROIC. The performance of the CBIRD FPA was reported previously [20]. ISC0903 operates in a sequential two-color mode n-on-p and then followed by a p-on-n or vice versa. It can also operate in just a single color mode in either n-on-p or p-on-n. After hybridization, the FPA was epoxy back-filled, and the substrate was removed. The FPA was mounted and wire-bonded to a standard 84-pin ceramic leadless chip carriers (LCC) and was loaded into the SEIR LN2 pour fill dewar with an f/4 cold-stop for testing and characterization. The dewar window has a broad spectral band that spans from 2 to 12  $\mu\text{m}$ ; there is no additional filter along the optical path.



**Fig 6. NEΔT histogram of n-type CBIRD FPA operating at 80 K temperature at a bias of 304 mV. The mean and median NEΔT are 18 mK and 17 mK at 1.86 msec integration time.**

NEΔT by definition is target to background minimum contrast temperature difference that results to a signal-to-noise ratio of unity. 124 sequential frames were collected at 22 °C, 27 °C and 32 °C flat black body temperatures. The responsivity matrix (R) was estimated from the difference of the temporal averages of many frames at 22 °C and at 32 °C and the temporal noise current matrix ( $I_{\text{noise}}$ ) was estimated from many frames at 27 °C. The temporal NEΔT is numerically evaluated using the relation,  $\text{NE}\Delta T = I_{\text{noise}}\Delta T/R$  [13] where  $\Delta T$  is 10 K. Figure 6 shows the NEΔT histogram

|   | NE $\Delta$ T > 40 mK Outliers | I <sub>noise</sub> > 1x10 <sup>-12</sup> A Outliers | R < 2.2x10 <sup>-11</sup> A/K Outliers |
|---|--------------------------------|---|--|
| NE $\Delta$ T > 40 mK Outliers                      | 737                            | 460   | 379                                    |
| I <sub>noise</sub> > 1x10 <sup>-12</sup> A Outliers | 460                            | 820   | 116                                    |
| R < 2.2x10 <sup>-11</sup> A/K Outliers              | 379                            | 116   | 829                                    |

**Table I. Diagonal elements are the pixel counts of outliers for NEDT, I<sub>noise</sub>, and R. Off diagonal elements are the pixels counts of logical “AND” operation on NEDT with I<sub>noise</sub>, NEDT and NEDT with R. The off diagonal element are pixels that are in common in both NEDT with I<sub>noise</sub>, NEDT and NEDT with R.**

of the CBIRD FPA operating at 80 K temperature. The mean and median NE $\Delta$ T at 304 mV bias and 1.86 msec integration time are 18 mK and 17 mK, respectively. The NE $\Delta$ T histogram is not symmetric and exhibits a tail, the origin of which requires further investigation. Fig 7(a) and Fig 7(b) show the estimated I<sub>noise</sub> (A) and R (A/°K) histogram and the tails in the distributions are clearly observable. The median I<sub>noise</sub> and R are  $\sim 5.1 \times 10^{-13}$  A and  $\sim 3.0 \times 10^{-11}$  A/°K, respectively. The ratio of I<sub>noise</sub> and R is related to NE $\Delta$ T and a tail can result if either the noise is large or the responsivity is small.

The tail origin in the NE $\Delta$ T is not entirely due to the tail on I<sub>noise</sub> histogram. To show this, first the total number and location of pixels with values greater than > 40 mK threshold are counted and recorded from NE $\Delta$ T matrix; total number and location of pixels with I<sub>noise</sub> > 1x10<sup>-12</sup> A threshold are counted and recorded and the total number and location of pixels with the R < 2.2x10<sup>-11</sup> A/K threshold are also counted and recorded. The reason is that the ratio of higher I<sub>noise</sub> and lower R can lead to NE $\Delta$ T tail. Secondly a binary (“1” or “0” value) images are constructed for pixel location which exceeds the threshold. A value of “1” means above (NE $\Delta$ T and I<sub>noise</sub>) or below (R) threshold and are considered outliers. Thirdly, a logical “AND” operation in the binary images of NE $\Delta$ T, with either I<sub>noise</sub> or R assures that the same pixel must appear in both binary images to produce a logical “1” result.[21] This is how the location of outliers are correlated from the two unrelated binary images. The diagonal elements in Table I enumerates the total number of pixels outliers for NE $\Delta$ T > 40 mK, I<sub>noise</sub> > 1x10<sup>-12</sup> A and R < 3.0x10<sup>-11</sup> A/°K. A logical “AND” operation of the same binary image will produce the same binary image and the number of “1”s in the resulting image is counted. This operation can be visualized as a spatial autocorrelation of the two similar binary images. The sum of all “1” in the resultant binary image is the total number of outlier pixels that the two binary images have in common. The off-diagonal elements in Table I are the pixels counts of a logical “AND” operation of NE $\Delta$ T outliers with either R or I<sub>noise</sub> outliers. The off-diagonal elements in Table I example is a NE $\Delta$ T AND’ed with I<sub>noise</sub> to detect the common outlier pixels at the same location for both binary images. This is the spatial correlation of outliers originated from two different conditions. I<sub>noise</sub> and R threshold were chosen to produce outlier count that exceeds the count of NE $\Delta$ T outlier. The interesting result is that some noisy pixels do not belong to the NE $\Delta$ T histogram tail. Similarly, lower R value pixels also do not belong to the NE $\Delta$ T histogram tail. These is demonstrated as the off-diagonal elements in Table I. An “AND” operations on the three binary images, NE $\Delta$ T, I<sub>noise</sub> and R, only resulted to a 492 pixels in common which is smaller than the 737 pixels NE $\Delta$ T outlier. However a logical “OR” on I<sub>noise</sub> and R and then the outcome is logically “ANDed” with NE $\Delta$ T outliers result in 723 pixels in common, which

is very close to the total number of pixels with  $NE\Delta T > 40$  mK (tail on the  $NE\Delta T$  histogram). A logical “OR” operation on two binary images results in combining all the “1” locations to a single binary image without double counting. By changing the threshold to  $5 \times 10^{-13}$  A for  $I_{\text{noise}}$  and  $3 \times 10^{-11}$  A/K for R, the number of pixels in common for either  $I_{\text{noise}}$  and R comes close to 737 pixels outliers for  $NE\Delta T > 40$  mK. However a logical “OR” on I and R and an “AND” with  $NE\Delta T$  result in 737 pixels in common, and it is equal to the total number of pixels with  $NE\Delta T$  above  $> 40$  mK of the  $NE\Delta T$  histogram. This means higher noise in  $I_{\text{noise}}$  is not the only determining factor for the appearance of a tail in the  $NE\Delta T$  histograms, but lower values of R is also a contributing factor to the appearance of tail in  $NE\Delta T$  histogram.

For  $1/f$  low frequency noise study, the method of data collection is similar to the nBn FPA. However, instead of the FPA staring at a constant temperature black body, the aperture is completely blocked. The low emissivity blocking material is made of shiny aluminum which is at the same temperature as the n-type CBIRD FPA. Therefore the CBIRD  $1/f$  noise study has no external influence from temperature fluctuation originating from either the window or the flat black body. Essentially this investigation focuses on the  $1/f$  noise behavior of dark current only.

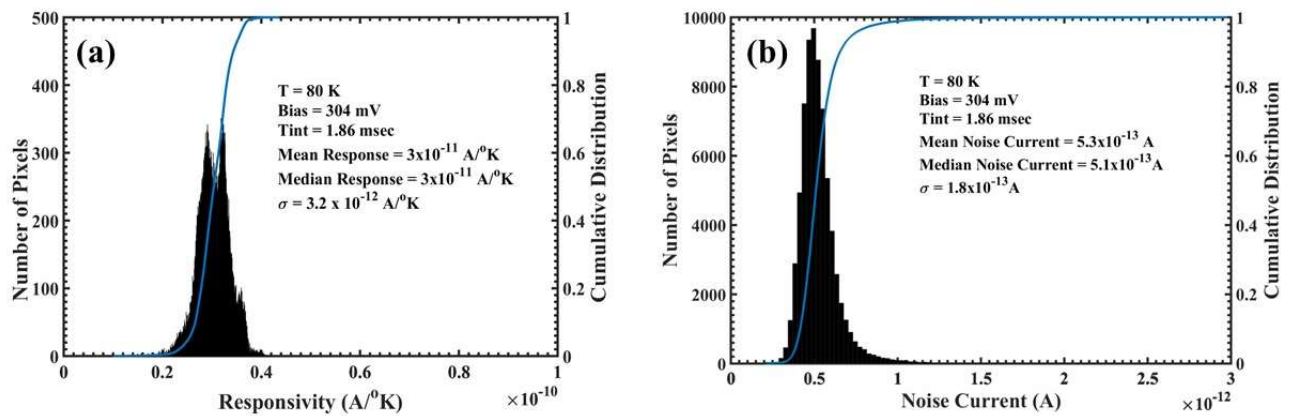


**Fig 7. (a) Responsivity histogram of the n-type CBIRD. (b) Noise current histogram of the n-type CBIRD**

An SEIR test system electronics was used to configure and electrically operate the CBIRD FPA. The temperature was kept at 80 K and the electronics system was allowed to warm up for at least one hour. The detector-on bias and integration time were set at 304 mV and 1.86 msec, respectively. The detector off and integration time were set at 0 mV and 1.86 msec, respectively. For this experiment, the FPA is operated in two color mode. However, instead of switching between n-on-p and p-on-n mode, the mode was kept the same at n-on-p mode only. That is, n-on-p mode but at two different biases. In one mode the bias is set at 304 mV n-on-p mode and in the other mode the bias is set at 0 V n-on-p mode. The data captured were done sequentially. The advantage in operating in the same mode but at two different biases is that the detector on and detector off frames are captured semi-simultaneously with a time difference approximately the inverse of the frame rate  $\sim 50$  msec. This is much smaller than the sampling time. The operating parameters are: frame rate = 20 Hz, Integration time = 1.86 msec, and FPA temperature = 80 K, and sampling interval is  $\Delta t = 10$  seconds.

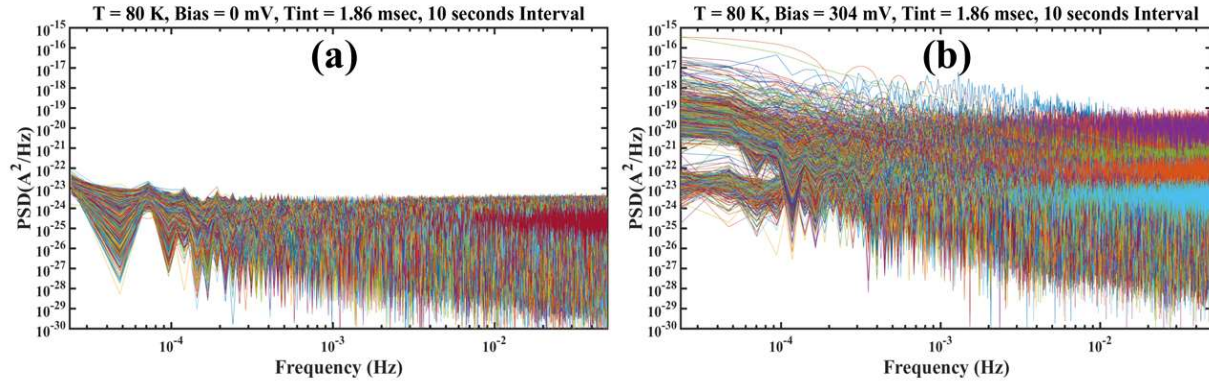


**Figure 8. (a) Detector off PSD of CBIRD FPA. (b) Detector on PSD of CBIRD FPA. The vertical scale scales on (a) and (b) are intentionally matched to illustrate the large PSD difference between detector off and detector on.**

It was discovered previously that PSD( $f$ ) estimates from the spatial mean of region of interests in time domain depends on size or number of contiguous pixels. To overcome this issue, the time series data are constructed for each pixel and spatial averaging is done in the frequency domain at the same frequency. This approach increases considerably the number of Fast Fourier transforms needed to compute all the PSDs. To sample a larger number of pixels and larger area, the PSD( $f$ ) calculations were conducted for the odd column and row only and this can be represented by PSD( $f,i,j$ ) distribution for the entire array, where  $i$  and  $j$  stand for a row and column index. The advantage here is that the PSD( $f,i,j$ ) provides a histogram distribution as function of frequency. Since there is a strong PSD cross correlation between adjacent neighbors, this approach (odd rows and columns) reduces the number of FFT operations, but the result still represents the FPA PSDs as a function of frequency and pixel location. Essentially the investigation focus on the  $1/f$  noise behavior at low frequency and white noise at high frequency of the dark current.

Fig. 8 (a) and (b) show the PSD for detector off and detector on respectively of odd rows and columns pixels. The vertical scales have been matched to demonstrate the large differences in PSDs between detector off and detector on. The detector off PSD contribution comes mostly from the system and since the detector is not the major source of noise, the ROIC is assumed the major noise contributor and input referred noises from external pre-amplifiers are assumed negligible. The ROIC noise can originate mostly from reset transistors.[13] The detector on PSD has higher PSD values than detector off PSD and has clustering at very low frequency. There are clustering at low frequency where one group has higher noise PSD than other group. This interesting clustering result would not have been observed if the data collection had a short time duration. Generally the noise level has increased when the detector is on. For comparison detector off does not show large spread and clustering. However, there are detector on pixels which have high frequency PSD  $\sim 10^{-24}$  A<sup>2</sup>/Hz comparable to detector off PSD.

Fig. 9 (a) and (b) show PSD( $f$ ) distribution at two fixed frequencies from Fig. 8 (a) and (b). The two frequencies are  $2.4 \times 10^{-5}$  Hz (red plot) and  $4.8 \times 10^{-2}$  Hz (blue plot) for detector on and detector off. This frequency range spans the lowest and highest frequencies that was determined from the captured data. These plots clearly show that for many pixels the PSD at lower frequencies are

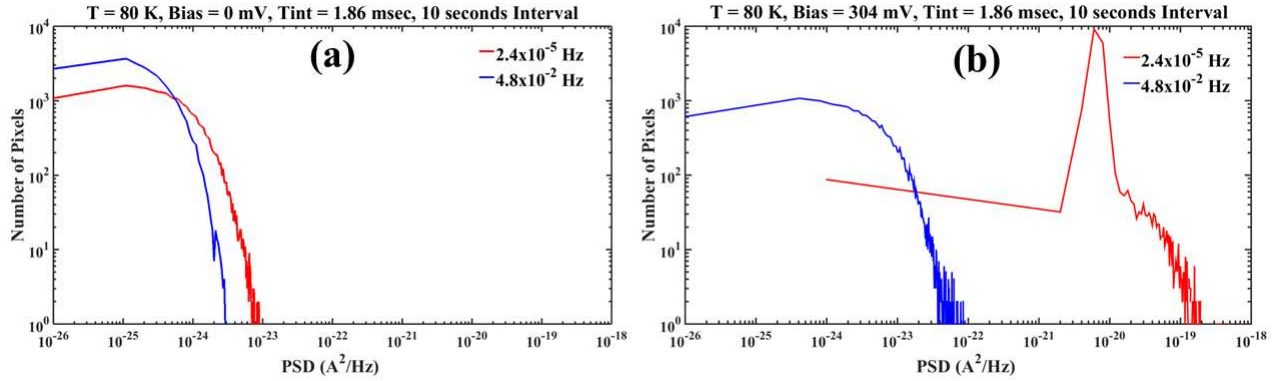


**Fig. 9** PSD distribution at two fixed frequencies for (a) Detector off, and (b) Detector on.

larger than the white noise at higher frequencies. In Fig. 9(a) detector off results show that at  $4.8 \times 10^{-2}$  Hz (blue plot), the noise PSD is low ( $< 7 \times 10^{-24}$  A<sup>2</sup>/Hz). At  $2.4 \times 10^{-5}$  Hz (red plot) the noise PSD is higher than  $> 7 \times 10^{-24}$  A<sup>2</sup>/Hz for some pixels. For PSD  $< 10^{-24}$  A<sup>2</sup>/Hz the number of pixels for  $2.4 \times 10^{-5}$  Hz (red plot) is lower than  $4.8 \times 10^{-2}$  Hz (blue plot) because many pixels have acquired extra noise. In Fig. 9(b) the detector on results show a similar trend. The detector on at high frequency  $\sim 4.8 \times 10^{-2}$  Hz (blue plot) has lower noise (PSD  $< 1 \times 10^{-22}$  A<sup>2</sup>/Hz) than the detector on at low frequency  $\sim 2.4 \times 10^{-5}$  Hz (red plot); it shows that most of the pixels acquired larger noise (PSD  $> 10^{-22}$  A<sup>2</sup>/Hz). Clearly these plots in Fig. 9(a) and 9(b) show that lower frequencies PSD is larger than the higher frequencies PSD for many pixels. This seems to be true for both the detector on and detector off PSD, although noise origin and magnitude are different.

Fig. 10 (a) shows the median PSD(f) for detector on and detector off. The detector off median PSD is related to the system noise power contribution as a function of frequency, and the detector on PSD is assumed to be the sum of the PSDs of the system and detector. However for detector on PSD, it is assumed that the contribution comes from detector dark current, which is significant at frequency below the  $f_c$  ( $\sim 10$  mHz). This  $f_c$  is higher than QWIP detector but it is lower than the  $f_c$

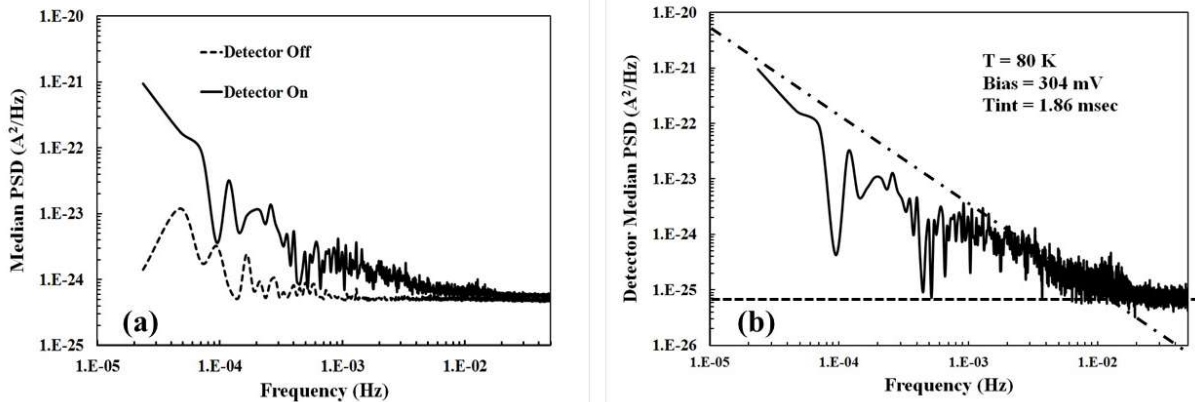


**Fig. 10.** (a) Median PSD of detector off and detector on. (b) Median PSD of CBIRD detector which is the difference between detector off and detector on PSDs from (a). The corner frequency of the detector only  $\sim 10$  mHz.

for the nBn detector. At higher frequencies, detector on PSD is only slightly higher than detector

off PSD. It is interesting to note that the detector on  $f_c$  ( $\sim 10^{-2}$  Hz) is roughly two orders of magnitude higher than the detector off  $f_c$  ( $\sim 4 \times 10^{-4}$  Hz). This implies either the  $f_c$  from the system is lower, or the  $f_c$  of detector is bias dependent where bias has shifted the  $f_c$  to higher frequency. The difference of median PSDs at each frequency of the detector on and detector off is shown in Fig. 10 (b). The PSD increases by two orders of magnitude between  $f_c \sim 10^{-2}$  Hz and  $10^{-4}$  Hz. A fit to PSD(f) of the form  $\sim \beta/f^\alpha$  gives a best fit parameters  $\beta \sim 10^{-27}$  A<sup>2</sup> and  $\alpha \sim 1$  below  $f_c$ . Above  $f_c$  the detector seems white noise limited. This low frequency  $1/f$  noise behavior is believed to be surface-related [16]. The CBIRD detector low frequency PSD is a good representation of the true noise power density because the external influence is suppressed. In addition, there is no large time delay in capturing the detector on and detector off data.

## Summary

Table II summarizes the result of low frequency noise measurement of the three FPAs. NE $\Delta$ T measurement actually has smaller noise bandwidth, higher operating frequency and hence does not capture low frequency noise. For very low frequency noise, measurement method was to capture frames at longer time interval. This allows for less data storage requirement. The time interval  $\Delta T$  is listed in Table II for each FPA tested. It is interesting to observe that NE $\Delta$ T values are decreasing as the cutoff wavelengths increases and as the integration time decreases. The corner frequency  $f_c$  shows an increasing trend with increasing quantum efficiency. The  $f_c$ 's in II-VI based FPAs have higher values compared to III-V based FPAs. A lower  $f_c$ 's frequency is good performance metric for an FPA because it implies stability of calibration matrix. That is, it requires longer time interval to re-calibrate the FPA.

For the n-type CBIRD, the tail on the NE $\Delta$ T was investigated by examining the noise current and the responsivity matrices. The outlier's pixels from NE $\Delta$ T tail with values  $> 40$  mK are counted and location recorded. By correlating the position of higher noise current pixel and low responsivity with the position NE $\Delta$ T outliers, it is found that not all higher noise current pixels contribute to the tail. It is found also that low responsivity can also contribute to the tail in NE $\Delta$ T. The  $f_c$ 's of detector off and detector on are different which seems to indicate a bias dependent  $f_c$ . This requires future investigation. The best fit to the PSD  $\sim 1/f^\alpha$  at low frequency below the  $f_c$  resulted to  $\alpha \sim 1$  which shows that it is a  $1/f$  noise.

Table II. Summary of low frequency noise measurement for a QWIP, an nBn, and a CBIRD FPA.

| Detector                            | QWIP Camera         | nBn IDCA            | n-type CBIRD LN2 Dewar |
|-------------------------------------|---------------------|---------------------|------------------------|
| ROIC                                | FLIR/Indigo ISC9803 | FLIR/Indigo ISC9803 | FLIR/Indigo ISC0903    |
| Temperature (K)                     | 65                  | 120                 | 80                     |
| Bias (Volt)                         | 1.6                 | 0.2                 | 0.304                  |
| Integration Time (msec)             | 16                  | 7.52                | 1.86                   |
| Quantum Efficiency (%)              | < 2                 | 67                  | 50                     |
| Cutoff Wavelength ( $\mu\text{m}$ ) | 6.2                 | ~ 4                 | 8.8                    |
| NEDT (mK)                           | 25                  | 15.6                | 17                     |
| $\Delta T$ interval (sec)           | 40                  | 2                   | 10                     |
| Corner Frequency $f_c$ (mHz)        | 0.5                 | 50-90               | 10                     |

## ACKNOWLEDGMENT

The authors thank M. Tidrow and S. Bandara of the U.S. Army Night Vision Electronics Sensor Directorate. The research described in this paper was carried out at the Jet Propulsion Laboratory, California Institute of Technology, through an agreement with the National Aeronautics and Space Administration. ©2017 California Institute of Technology. Government sponsorship acknowledged."

## REFERENCES

- 1) Hui Tian, Boyd Fowler, and Abbas El Gamal, Analysis of Temporal Noise in CMOS APS, SPIE. Vol. 3649 1999.
- 2) Igor Brouk, Amikam Nemirovsky, Kamal Alameh, Yael Nemirovsky, Analysis of noise in CMOS image sensor based on a unified time-dependent approach, Solid State Electronics 54 (2010) 28-36.
- 3) A. I. D'Souza, M. G. Stapelbroek, P. S. Wijewarnasuriya, R. E. DeWames, and G. M. Williams, "1/f Noise in Very-Long-Wavelength Infrared  $\text{Hg}_{1-x}\text{Cd}_x\text{Te}$  Detectors", Journal of Electronic Materials, Vol. 31, pp. 699-704 (2002).
- 4) Soo Ho Bae, Sang Jun Lee, Young Ho Kim, Hee Chul Lee, and Choong Ki Kim, Analysis of 1/f Noise in LWIR in LWIR  $\text{HgCdTe}$  Photodiode, Journal of Electronic Materials, Vol. 29, No.6, 2000.
- 5) J. B. Johnson, "The Schottky Effect in Low Frequency Circuits" Phys. Rev. 26, pp. 71-85 (1925).
- 6) Luca Calegari, "Electrical Impedance Principles, Measurement, and Applications", CRC Press, 2013.
- 7) Arnold Daniels, Field Guide to Infrared Systems, Detectors, and FPAs, 2<sup>nd</sup> ed. 2007.
- 8) Cornelius J. Willers, "Electro-Optical System Analysis and Design A Radiometric Perspective", SPIE Press, 2013.
- 9) Majeed M. Hayat, Sergio N. Torres, Ernest Armstrong, Stephen C. Cain, and Brian Yasuda, Statistical algorithm for nonuniformity correction in focal plane arrays, APPLIED OPTICS, Vol. 38, No. 8, 10 March 1999.

- 10) F. N. Hooge, "1/f Noise Sources", IEEE Transactions on Electron Devices, 41, 1926-1935 (1994).
- 11) A. van der Ziel, Advances in Electronics and Electron Physics (Edited by L. Martin) pp.225-297. Academic Press, New York (1979).
- 12) Alan V. Oppenheim and Ronald W. Schaffer, "Digital Signal Processing", Prentice Hall, 1975.
- 13) Hui Tian, Boyd Fowler, and Abbas El Gamal, Analysis of Temporal Noise in CMOS APS, SPIE Vol. 3649, 1999.
- 14) Michael E. Ressler, James J. Bock, Sumith V. Bandara, Sarath D. Gunapala, Astronomical imaging with quantum well infrared photodetector, Infrared Physics & Technology 42, 2001.
- 15) S. Maimon and G. W. Wicks, "nBn detector, an infrared detector with reduced dark current and higher operating temperatures", Applied Physics Letters, vol. 89, pp. 151109-1 to 151109-3, 2006.
- 16) Alexander Soibel, David Z.-Y. Ting, Cory J. Hill, Mike Lee, Jean Nguyen, Sam A. Keo, Jason M. Mumolo, and Sarath D. Gunapala, "Gain and noise of high-performance long wavelength superlattice infrared detectors" Appl. Phys. Lett. **96**, 111102 (2010).
- 17) D. Z.-Y. Ting, C. J. Hill, A. Soibel, S. A. Keo, J. M. Mumolo, J. Nguyen, and S. D. Gunapala, "A high-performance long wavelength superlattice complementary barrier infrared detector", *Appl. Phys. Lett.* **95**, 023508 (2009).
- 18) D. Z.-Y. Ting, A. Soibel, A. Khoshakhlagh, J. Nguyen, L. Höglund, S. A. Keo, J. M. Mumolo, and S. D. Gunapala, "Exclusion, extraction, and junction placement effects in the complementary barrier infrared detector", *Appl. Phys. Lett.* **102**, 121109 (2013).
- 19) B. Simolon, A. Aziz, R. Hansen, E. Kurth, S. Lam, S. Petronio, and J. Woolaway, "Standard format two-color CMOS ROIC for SLS detectors", Proceedings of the International Conference on Quantum Structure Photodetectors(QSIP) 2010, Infrared Physics & Technology 54 (2011) 306-309.
- 20) Sir B. Rafol, Alexander Soibel, Arezou Khoshakhlagh, Jean Nguyen, John K. Liu, Jason M. Mumolo, Sam A. Keo, Linda Hoglund, David Z. Ting, Sarath D. Gunapala, "Performance of a 1/4 VGA Format Long-Wavelength Infrared Antimonides Based Superlattice Focal Plane Array, IEEE Journal of Quantum Electronics, Vol. 48, Issue 7, 2012.
- 21) Milan Sonka, Vaclav Hlavac, Roger Boyle, "Image Processing, Analysis, and Machine Vision, Brooks/Cole Publishing Inc. 1999.